Deterministic linear-optical quantum control gates utilizing path and polarization degrees of freedom

Hongyi Meng*
Department of Physics, The University of Chicago, Chicago, Illinois 60637, USA

(Received 1 October 2020; accepted 23 February 2022; published 10 March 2022)

We present a general scheme for a family of linear-optical quantum control gates, including controlled-NOT and controlled-SWAP gates for two or three qubits. Our approach utilizes polarization-path-entangled pairs of photons and encodes qubits in mixed degrees of freedom with the control qubit specifically occupying the polarization degree of freedom. By exploiting multiple degrees of freedom and initial state entanglement of the two photons, the proposed control gates do not require any ancilla photons or measurement-induced nonlinearities. Since our gates are purely linear and we implicitly use nonlinearities in a standard manner to create entanglement via parametric nonlinear process, our work demonstrates that a need to have nonlinearities in the photonic gates can be shifted to the state preparation stage; the cost of such shift is that the construction of a certain class of single-qubit operations, such as Hadamard, needs to be probabilistic. In particular, we focus on a deterministic linear-optical quantum Fredkin (controlled-SWAP) gate and perform a full characterization of the gate performance with a high fidelity typically well above 99% under realistic conditions. The proposed control gates rely on simple linear-optical elements and polarization-entangled photon pairs readily generated from ubiquitous sources, making the gates experimentally feasible with current technologies.

DOI: 10.1103/PhysRevA.105.032607

I. INTRODUCTION

Quantum computing [1] is a sought-after technique to redefine computation and tackle problems unsolvable by the best classical computers. Recently, Google claimed the quantum supremacy [2], but the superconducting qubit processors suffer from the loss of quantum coherence and the difficulty of scalability while using expensive cryogenic implementation strongly coupling to the environment. On the other hand, photonic technologies serve already relatively affordable solutions, and photonic qubits are well suited both for low-decoherence applications and for carriers that transmit quantum information.

Linear optics implementations [3–5] play a prominent role in various quantum information processing schemes due to the relative ease of manipulating quantum states of photons, as compared to the trapped ions [6] or superconducting qubits [7]. In 2001, Knill *et al.* [8] revolutionized the field by showing that efficient quantum computing is possible using only linear-optical components such as beam splitters and phase shifters. Since then, several groups have proposed and demonstrated various linear-optical quantum gates.

In recent years, quantum gates have been demonstrated in a number of different photonic degrees of freedom (DoFs) [9–12]. Among all these degrees of freedom, the spatial and polarization DoFs appear frequently due to the relative ease to encode and process quantum information. By exploiting multiple DoFs and thereby increasing the capacity of the quantum information carried, we will be able to sidestep some probabilistic multiphoton interactions. Deterministic quantum information processors for systems with several degrees of freedom of a single photon [13–15] have been demonstrated; for example, upon entangling a spatial binary alternative of a photon with its polarization by the use of free-space optics associated with single-photon interferometry, one can use single photons to study arbitrary two-qubit states [16].

A set of quantum logical gates is said to be universal if any unitary operation on n qubits may be implemented by a quantum circuit involving only those gates [1]. Quantum control gates are sufficient for universal quantum computing, since controlled-NOT, controlled-SWAP, or any other entangling two-qubit gate, along with single-qubit gates, are universal for quantum computation [17,18]. In this paper, we propose a general scheme for constructing a family of entanglement-based control gates, and the three-qubit controlled-SWAP (Fredkin) gate is a nontrivial example that illustrates the essence of our proposal. The quantum Fredkin gate is a computational circuit suitable for reversible computing: conditioned on the state of the control qubit, the quantum states of the two target qubits are swapped. The first design of the quantum Fredkin gate [19] was realized with single-photon optics by exploiting the Cross-Kerr nonlinearities, yet it is difficult to achieve high nonlinearities [20]. Following the Knill-Laflamme-Milburn (KLM) protocol [8], new types of heralded probabilistic quantum Fredkin gates have been designed [21,22]. However, the probability of success decreases significantly as successive probabilistic gates are applied. Our strategy is to encode quantum information in both the spatial and polarization degrees of freedom of two polarization-entangled photons. While our proposal is similar to a number of schemes [23–25] demonstrating linear-optical CNOT gates

*menghongyi@uchicago.edu

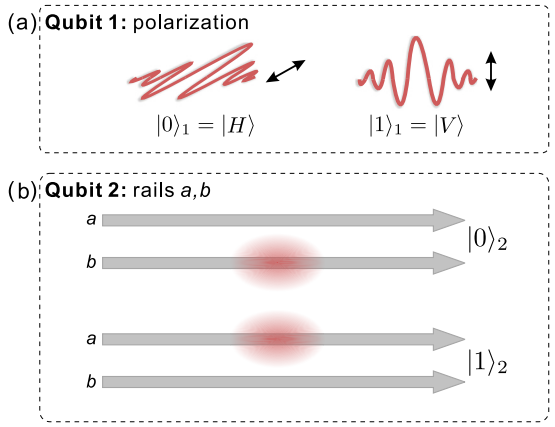

FIG. 1. (a) The first logical qubit is encoded in the polarization state of the photon. If the photon is horizontally polarized, the first logical qubit is $|0\rangle_1$; if it is vertically polarized, the first logical qubit is $|1\rangle_1$. (b) The second logical qubit is encoded in the spatial degree of freedom of the photon (which can occupy either spatial mode a or b). If it occupies spatial mode b, the second logical qubit is $|0\rangle_2$; otherwise, the second logical qubit is $|1\rangle_2$

involving multiple degrees of freedom of a single photon, here we report an implementation of a deterministic linear-optical Fredkin gate for two-photon three-qubit quantum logic. The experimental proposal does not require any ancilla photons and is experimentally feasible with current technology, leading to a simple and efficient way to implement a linear-optical controlled-SWAP gate.

II. THE CONTROLLED-NOT GATE

The general strategy for constructing linear-optical control gates in our scheme is to encode quantum information by accessing multiple degrees of freedom of a single photon or photon pairs, with the control qubit encoded in the polarization state and target qubit(s) encoded in the path. One notable example is the implementation of a linear-optical controlled-NOT gate. In this case, we will encode two-qubit quantum information utilizing the polarization and path of a single photon, as shown in Fig. 1.

Without any loss of generality, the input state of the controlled-NOT gate is given by

$$|\varphi_{\text{in}}\rangle = (\alpha|0\rangle_1 + \beta|1\rangle_1) \otimes (\gamma|0\rangle_2 + \delta|1\rangle_2), \tag{1}$$

where the coefficients $\alpha, \beta, \gamma, \delta$ are arbitrary complex numbers, satisfying the normalization condition $|\alpha|^2 + |\beta|^2 = |\gamma|^2 + |\delta|^2 = 1$.

The schematic for the state-preparation stage is shown in Fig. 2(a). Initially, the photon generated by a single-photon source will occupy spatial mode b,

$$|\varphi\rangle = \alpha\hat{b}_H^\dagger|\text{vac}\rangle + \beta\hat{b}_V^\dagger|\text{vac}\rangle \tag{2}$$

where $\hat{b}^\dagger$ is the bosonic creation operator in spatial mode b. The label H or V indicates the polarization state of the photon, and $|\text{vac}\rangle$ denotes the vacuum state.

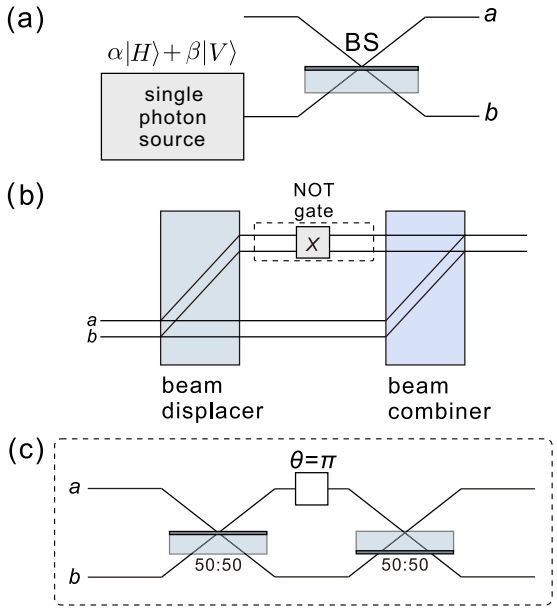

FIG. 2. (a) Experimental setup of the state-preparation stage. Initially, we have a single photon $|Q_1\rangle = \alpha|H\rangle + \beta|V\rangle = \alpha|0\rangle_1 + \beta|1\rangle_1$. Applying beam splitters on each output mode, we will be able to encode the second logical qubit in dual rail. The dual-rail qubit will be turned into state $|Q_2\rangle = \gamma|0\rangle_2 + \delta|1\rangle_2$ by reconfiguring the reflectivity and phase shifts of the beam-splitter coatings. (b) The physical implementation of the proposed controlled-NOT gate. Note that the calcite beam combiner is the same as the calcite beam displacer, but rotated by 90 degrees to keep the symmetry of the two arms. (c) A Mach-Zehnder interferometer with an inner phase π performs an optical switching between two spatial modes, which acts as the NOT gate on the target qubit.

The evolution of the initial state as it interferes on the beam splitter can be modeled as

$$\hat{b}_\sigma^\dagger \xrightarrow{\hat{U}_{\text{BS}}} \delta\hat{a}_\sigma^\dagger + \gamma\hat{b}_\sigma^\dagger, \tag{3}$$

where $\sigma = H, V$ signals the polarization property of the photon. The coefficients δ and γ are determined by the transmission and reflection property of the beam splitter and can therefore be adjusted arbitrarily. The quantum state after the beam splitters is then

$$|\varphi\rangle \to \alpha(\delta\hat{a}_H^\dagger + \gamma\hat{b}_H^\dagger)|\text{vac}\rangle + \beta(\delta\hat{a}_V^\dagger + \gamma\hat{b}_V^\dagger)|\text{vac}\rangle. \tag{4}$$

Therefore, the quantum state after the state preparation stage is

$$|\varphi_{\text{in}}\rangle = (\alpha\delta\hat{a}_H^\dagger + \alpha\gamma\hat{b}_H^\dagger + \beta\delta\hat{a}_V^\dagger + \beta\gamma\hat{b}_V^\dagger)|\text{vac}\rangle, \tag{5}$$

which, by the definition of our logical qubits, corresponds to the general input state

$$|\varphi_{\text{in}}\rangle = \alpha\gamma|00\rangle + \alpha\delta|01\rangle + \beta\gamma|10\rangle + \beta\delta|11\rangle. \tag{6}$$

Note that (6) is just the expanded version of the general input state in (1).

The proposed controlled-NOT gate consists of two noncentrosymmetric calcite crystals and a NOT gate on the target qubit, as shown in Fig. 2(b). The calcite beam displacer will orient the photon into either the upper or lower arm based on the polarization states of the photon, and the calcite beam

combiner will recombine the two paths. If the control qubit is in state $|1\rangle_1$, which suggests the photon is vertically polarized, a NOT operation will be applied on the target qubit. The NOT gate on the target qubit consists of a Mach-Zehnder interferometer with an internal phase ϕ, as shown in Fig. 2(c). The Mach-Zehnder interferometer is characterized by the following mode transformation matrix:

$$\hat{U} = \frac{1}{\sqrt{2}}\begin{pmatrix} 1 & i \\ i & 1 \end{pmatrix}\begin{pmatrix} e^{i\phi} & 0 \\ 0 & 1 \end{pmatrix}\frac{1}{\sqrt{2}}\begin{pmatrix} 1 & -i \\ -i & 1 \end{pmatrix}, \tag{7}$$

$$\hat{U} = e^{i\frac{\phi}{2}}\begin{pmatrix} \cos\frac{\phi}{2} & -\sin\frac{\phi}{2} \\ \sin\frac{\phi}{2} & \cos\frac{\phi}{2} \end{pmatrix}. \tag{8}$$

By substituting $\phi = \pi$ and ignoring the global phase, the above matrix will become the Pauli X matrix and perform an optical switching between two input spatial modes. Note that the second 50:50 beam splitter is flipped with respect to the first 50:50 beam splitter and their corresponding mode transformation matrices are slightly different.

If the photon is vertically polarized, the quantum CNOT gate will act nontrivially; in such case, the following two transformations are naturally implemented:

$$\hat{a}_V^\dagger \to \hat{b}_V^\dagger, \hat{b}_V^\dagger \to \hat{a}_V^\dagger. \tag{9}$$

After the quantum Fredkin gate, the superposition state in (5) becomes

$$|\varphi_{\text{out}}\rangle = (\alpha\delta\hat{a}_H^\dagger + \alpha\gamma\hat{b}_H^\dagger + \beta\delta\hat{b}_V^\dagger + \beta\gamma\hat{a}_V^\dagger)|\text{vac}\rangle, \tag{10}$$

which corresponds to the output state,

$$|\varphi_{\text{out}}\rangle = \alpha\gamma|00\rangle + \alpha\delta|01\rangle + \beta\gamma|11\rangle + \beta\delta|10\rangle. \tag{11}$$

III. THE CONTROLLED-SWAP GATE

Another notable example in our proposal is the implementation of a linear-optical controlled-SWAP gate. In this case, we have to encode three-qubit quantum information utilizing the polarization and path of a photon pair, as shown in Fig. 3.

Without any loss of generality, the input state of the quantum Fredkin gate is given by

$$|\varphi'_{\text{in}}\rangle = (\alpha|0\rangle_1 + \beta|1\rangle_1) \otimes (\gamma|0\rangle_2 + \delta|1\rangle_2) \otimes(\mu|0\rangle_3 + \nu|1\rangle_3), \tag{12}$$

where the coefficients $\alpha, \beta, \gamma, \delta, \mu, \nu$ are arbitrary complex numbers, satisfying the normalization condition $|\alpha|^2 + |\beta|^2 = |\gamma|^2 + |\delta|^2 = |\mu|^2 + |\nu|^2 = 1$.

At present, there exist a number of entangled photon generation schemes including spontaneous parametric down-conversion (SPDC) [26] in a noncentrosymmetric crystal and spontaneous four-wave mixing (SFWM) in an optical fiber [27]. The complete process of generating entangled photon pairs $|\varphi\rangle = \alpha|HH\rangle + \beta|VV\rangle$ via frequency-degenerate type-I SPDC pumped by a continuous wave laser in noncollinear regimes is discussed in [26]. An alternative method utilizing type-II SPDC from a round-trip configuration of a double-pass polarization Sagnac interferometer is presented in [28].

The schematic for state-preparation stage is shown in Fig. 4(a). Initially, the two photons will occupy spatial modes b and c, and they are guaranteed to have the same polarization.

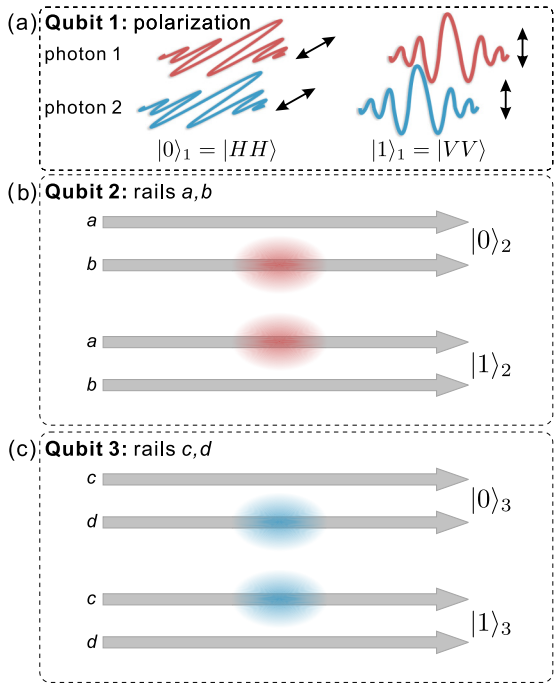

FIG. 3. (a) The first logical qubit is encoded in the polarization state of the photon pair. If the photons are horizontally polarized, the first logical qubit is $|0\rangle_1$; if the photons are vertically polarized, the first logical qubit is $|1\rangle_1$. Here, we use two colors to distinguish the two photons in our scheme. Note that they should be ideally indistinguishable in all degrees of freedom except the rails. (b) The second logical qubit is encoded in spatial degree of freedom of the first photon (which can occupy either spatial mode a or b). If it occupies spatial mode b, the second logical qubit is $|0\rangle_2$; otherwise, the second logical qubit is $|1\rangle_2$. (c) Similarly, the third logical qubit is encoded in the spatial degree of freedom of the second photon.

Therefore, the initial state is

$$|\varphi'\rangle = \alpha\hat{b}_H^\dagger\hat{c}_H^\dagger|\text{vac}\rangle + \beta\hat{b}_V^\dagger\hat{c}_V^\dagger|\text{vac}\rangle, \tag{13}$$

where $\hat{b}^\dagger$and $\hat{c}^\dagger$ are bosonic creation operators in spatial mode b and c, respectively, and the label H or V indicates the polarization state.

The evolution of the initial state as it interferes on beam splitters 1 and 2 can be modeled as follows:

$$\hat{b}_\sigma^\dagger \xrightarrow{\hat{U}_{\text{BS1}}} \delta\hat{a}_\sigma^\dagger + \gamma\hat{b}_\sigma^\dagger, \tag{14}$$

$$\hat{c}_\sigma^\dagger \xrightarrow{\hat{U}_{\text{BS2}}} \nu\hat{c}_\sigma^\dagger + \mu\hat{d}_\sigma^\dagger, \tag{15}$$

where $\sigma = H, V$ signals the polarization property of the photon. The quantum state after the beam splitters is then

$$|\varphi'\rangle \to \alpha\left(\delta\hat{a}_H^\dagger + \gamma\hat{b}_H^\dagger\right)\left(\nu\hat{c}_H^\dagger + \mu\hat{d}_H^\dagger\right)|\text{vac}\rangle + \beta\left(\delta\hat{a}_V^\dagger + \gamma\hat{b}_V^\dagger\right)\left(\nu\hat{c}_V^\dagger + \mu\hat{d}_V^\dagger\right)|\text{vac}\rangle. \tag{16}$$

Therefore, the superposition state after the state-preparation stage is

$$|\varphi'_{\text{in}}\rangle = (\alpha\delta\nu\hat{a}_H^\dagger\hat{c}_H^\dagger + \alpha\delta\mu\hat{a}_H^\dagger\hat{d}_H^\dagger)|\text{vac}\rangle + (\alpha\gamma\nu\hat{b}_H^\dagger\hat{c}_H^\dagger + \alpha\gamma\mu\hat{b}_H^\dagger\hat{d}_H^\dagger + \beta\delta\nu\hat{a}_V^\dagger\hat{c}_V^\dagger)|\text{vac}\rangle + (\beta\delta\mu\hat{a}_V^\dagger\hat{d}_V^\dagger + \beta\gamma\nu\hat{b}_V^\dagger\hat{c}_V^\dagger + \beta\gamma\mu\hat{b}_V^\dagger\hat{d}_V^\dagger)|\text{vac}\rangle, \tag{17}$$

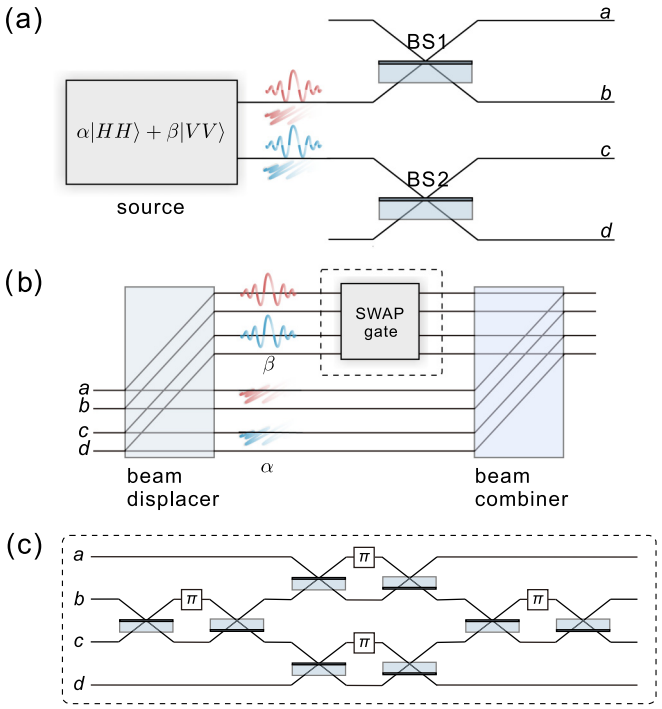

FIG. 4. (a) Experimental setup of the state-preparation stage. Initially, we have an entangled photon pair $|Q_1\rangle = \alpha|HH\rangle + \beta|VV\rangle = \alpha|0\rangle_1 + \beta|1\rangle_1$. The second and third dual-rail qubits will be turned into state $|Q_2\rangle = \gamma|0\rangle_2 + \delta|1\rangle_2$ and $|Q_3\rangle = \mu|0\rangle_3 + \nu|1\rangle_3$, respectively. (b) The physical implementation of the proposed controlled-SWAP gate. The calcite beam displacer will orient the two photons into either the upper or lower arm based on the polarization states. Note that the two photons will always go through either the upper or the lower arm together since they are guaranteed to have the same polarization state. (c) The physical implementation of the deterministic SWAP gate on the target qubits, which is composed of four successive Mach-Zehnder interferometers with an inner phase π. Note that all the beam splitters in the Mach-Zehnder interferometer should be ideal 50:50 beam splitters.

which, by the definition of our logical qubits, corresponds to the general input state

$$|\varphi'_{\text{in}}\rangle = \alpha\gamma\mu|000\rangle + \alpha\gamma\nu|001\rangle + \alpha\delta\mu|010\rangle + \alpha\delta\nu|011\rangle + \beta\gamma\mu|100\rangle + \beta\gamma\nu|101\rangle + \beta\delta\mu|110\rangle + \beta\delta\nu|111\rangle. \tag{18}$$

Note that (18) is just the expanded version of the general input state in (12).

The proposed quantum Fredkin gate consists of two noncentrosymmetric calcite crystals and a SWAP gate on the target qubits. The physical implementation of the quantum Fredkin gate is shown in Fig. 4(b). If the control qubit is in state $|0\rangle_1$, which suggests the two photons are horizontally polarized, an identity matrix is applied on the second and third logical qubits; otherwise, a SWAP operation

$$U_{\text{SWAP}} = \begin{bmatrix} 1 & 0 & 0 & 0 \\ 0 & 0 & 1 & 0 \\ 0 & 1 & 0 & 0 \\ 0 & 0 & 0 & 1 \end{bmatrix} \tag{19}$$

will be applied on the second and third qubits. The square bracket here denotes a state transformation matrix.

In our proposal, the deterministic swap gate on the target qubits consists of four successive Mach-Zehnder interferometers with an inner phase $\phi = \pi$, as shown in Fig. 4(c). Besides free space, the deterministic SWAP gate could also be readily implemented on-chip [29] by exploiting the distinction of the waveguide crossings.

If the two photons are both vertically polarized, the quantum Fredkin gate will act nontrivially; in such case, a deterministic SWAP operation is performed so that the following four transformations are naturally implemented:

$$\hat{a}_V^\dagger \to \hat{c}_V^\dagger, \quad \hat{c}_V^\dagger \to \hat{a}_V^\dagger, \quad \hat{b}_V^\dagger \to \hat{d}_V^\dagger, \quad \hat{d}_V^\dagger \to \hat{b}_V^\dagger. \tag{20}$$

After the quantum Fredkin gate, the superposition state in (16) becomes

$$|\varphi'_{\text{out}}\rangle = \alpha(\delta\hat{a}_H^\dagger + \gamma\hat{b}_H^\dagger)(\nu\hat{c}_H^\dagger + \mu\hat{d}_H^\dagger)|\text{vac}\rangle + \beta(\delta\hat{c}_V^\dagger + \gamma\hat{d}_V^\dagger)(\nu\hat{a}_V^\dagger + \mu\hat{b}_V^\dagger)|\text{vac}\rangle, \tag{21}$$

which corresponds to the output state

$$|\varphi'_{\text{out}}\rangle = \alpha\gamma\mu|000\rangle + \alpha\gamma\nu|001\rangle + \alpha\delta\mu|010\rangle + \alpha\delta\nu|011\rangle + \beta\gamma\mu|100\rangle + \beta\gamma\nu|110\rangle + \beta\delta\mu|101\rangle + \beta\delta\nu|111\rangle. \tag{22}$$

To understand the overall effect of the proposed circuit in Fig. 4(b), let us investigate, for example, the transformation obtained in the evolution of two input photons that are horizontally polarized and occupy spatial modes b and d. The input state in this case, by definition, is simply $|000\rangle$. The photons will be transmitted together through the calcite beam displacer and be deviated together by the calcite beam combiner. Both the polarization states and the spatial modes in which the two photons occupy are unchanged, so the output state is still $|000\rangle$. On the other hand, if the two input photons are vertically polarized and occupy spatial modes a and d, then the input state is $|110\rangle$. The two photons will be deviated together by the beam displacer and enter the deterministic SWAP gate. After the SWAP gate, the two photons will occupy spatial modes b and c. Finally, the two photons will be transmitted again through the beam combiner. The output state in this case is $|101\rangle$.

The basis states for the gate are $|000\rangle$, $|001\rangle$, $|010\rangle$, $|011\rangle$, $|100\rangle$, $|101\rangle$, $|110\rangle$, and $|111\rangle$, and they will span an eight-dimensional Hilbert space. If we consider the first logical qubit encoded in the polarization state as the control qubit and the second and third logical qubits encoded in dual rail as the target qubits in a controlled-SWAP (CSWAP) operation, with the experimental proposal above, the classical controlled-SWAP (CSWAP) transformations are naturally implemented,

$$U_{\text{CSWAP}} = \begin{bmatrix} 1 & 0 & 0 & 0 & 0 & 0 & 0 & 0 \\ 0 & 1 & 0 & 0 & 0 & 0 & 0 & 0 \\ 0 & 0 & 1 & 0 & 0 & 0 & 0 & 0 \\ 0 & 0 & 0 & 1 & 0 & 0 & 0 & 0 \\ 0 & 0 & 0 & 0 & 1 & 0 & 0 & 0 \\ 0 & 0 & 0 & 0 & 0 & 0 & 1 & 0 \\ 0 & 0 & 0 & 0 & 0 & 1 & 0 & 0 \\ 0 & 0 & 0 & 0 & 0 & 0 & 0 & 1 \end{bmatrix}. \tag{23}$$

The readout process is also simple, requiring only one polarizing beam splitter and eight non-photon-number-resolving detectors such as the avalanche photodiode (APD) [30], which offers low dark counts and reasonable quantum efficiency in an easy and affordable way. The proposed quantum Fredkin gate should be robust against photon loss because the photons are encoded in dual rail rather than single rail: the loss of a photon is easily noted by its absence. Even though the dual-rail encoded qubits are generally susceptible to path-length mismatch, different optical paths in our scheme are highly symmetric. In the end, we only accept detection events where precisely two photons appear on the same side of the polarizing beam splitter (that is, photons of the same polarization). In this section, we assume all the detectors are perfect, i.e., they have unit quantum efficiency and zero dark counts. In the next section, we will discuss errors introduced by realistic detectors.

IV. CHARACTERIZATION OF THE CONTROLLED-SWAP GATE

A. Imperfections due to the calcite beam displacer

When the photons enter the first calcite beam displacer, the deviation of mirror mounts θ and the polarization extinction ratio of the calcite beam displacer r will deviate the real quantum state from the perfect input state. Therefore, the mode transformation matrix acting on the two creation operators due to the imperfection is given by

$$\hat{U}_{\mathrm{BD}} = \hat{U}_{r_1}\hat{U}_\theta = \begin{pmatrix} \frac{1}{\sqrt{1+r}} & \frac{\sqrt{r}}{\sqrt{1+r}} \\ \frac{-\sqrt{r}^*}{\sqrt{1+r}} & \frac{1}{\sqrt{1+r}} \end{pmatrix} \begin{pmatrix} \cos\theta & \sin\theta \\ -\sin\theta & \cos\theta \end{pmatrix}, \quad (24)$$

$$\hat{U}_{\mathrm{BD}} \begin{pmatrix} \hat{\chi}_H^\dagger \\ \hat{\chi}_V^\dagger \end{pmatrix} = \frac{1}{\sqrt{1+r}} \times \begin{pmatrix} \cos\theta - \sqrt{r}\sin\theta & \sin\theta + \sqrt{r}\cos\theta \\ -\sqrt{r}^*\cos\theta - \sin\theta & -\sqrt{r}^*\sin\theta + \cos\theta \end{pmatrix} \begin{pmatrix} \hat{\chi}_H^\dagger \\ \hat{\chi}_V^\dagger \end{pmatrix}, \quad (25)$$

where $\chi = a, b, c, d$. Assume that the input state is $|\varphi_{\mathrm{in}}\rangle = |000\rangle = \hat{b}_H^\dagger \hat{d}_H^\dagger |\mathrm{vac}\rangle$; the fidelity is then given by

$$\mathcal{F}_1 = |\langle\varphi_{\mathrm{real}}|\varphi_{\mathrm{expected}}\rangle|^2 = \left|\frac{1}{1+r}(\cos\theta - \sqrt{r}\sin\theta)^2\right|^2. \quad (26)$$

The imperfections due to the calcite beam displacer will only affect the polarization state of the two photons since the spatial information is preserved at this stage. Thus, for input states $|001\rangle, |010\rangle, |011\rangle$, the fidelity calculated from the above procedures is the same as $\mathcal{F}_1$. Similarly, the fidelity for the input states $|100\rangle, |101\rangle, |110\rangle, |111\rangle$ is given by

$$\mathcal{F}_2 = \left|\frac{1}{1+r}(-\sqrt{r}^*\sin\theta + \cos\theta)^2\right|^2 = \mathcal{F}_1. \quad (27)$$

Partial distinguishability of the interfering photons can be modeled by assuming that at the input, the photon in the upper path occupies a certain mode $\hat{a}_1$, while the lower path photon is prepared in a combination of a matching mode $\hat{c}_1$ and another orthogonal mode $\hat{c}_2$, where the lower labels 1 and 2 denote different spectral information. Due to the imperfect indistinguishability of the two photons, the real input state is

$$|\varphi_{\mathrm{real}}\rangle = |011\rangle = \hat{a}_{H1}^\dagger(\sqrt{\mathcal{V}}\hat{c}_{H1}^\dagger + \sqrt{1-\mathcal{V}}\hat{c}_{H2}^\dagger)|\mathrm{vac}\rangle, \quad (28)$$

where $\mathcal{V}$ denotes the visibility measuring the indistinguishability between photons. When measured, the second part $\sqrt{1-\mathcal{V}}\hat{c}_{H2}^\dagger|\mathrm{vac}\rangle$ is often lost. In this case, the fidelity is given by

$$\mathcal{F}_1' = \mathcal{F}_2' = \left|\frac{\sqrt{\mathcal{V}}}{1+r}(-\sqrt{r}^*\sin\theta + \cos\theta)^2\right|^2. \quad (29)$$

Therefore, the imperfection due to partial distinguishability simply scales the fidelity by a factor of $\mathcal{V}$.

B. The crosstalk of the SWAP gate

For the input state $|100\rangle, |101\rangle, |110\rangle, |111\rangle$, the two photons will also go through the swap gate consisting of four successive Mach-Zehnder interferometers with internal phase $\phi = \pi$, which is characterized by the following mode transformation matrix in (7). If the real phase difference between the two arms of the Mach-Zehnder interferometer is $\phi = \pi - \Delta\phi$, the unitary mode transformation matrix that corresponds to the internal phase shifter becomes

$$\hat{U}_\phi = \begin{pmatrix} e^{i(\pi-\Delta\phi)} & 0 \\ 0 & 1 \end{pmatrix}. \quad (30)$$

If the transmission rate of the beam splitter deviates slightly from 50%, the unitary mode transformation matrix that corresponds to the two 50:50 beam splitters becomes

$$\hat{U}_{\mathrm{BS}} = \frac{1}{\sqrt{\epsilon^2+2\epsilon+2}} \begin{pmatrix} 1+\epsilon & i \\ i & 1+\epsilon \end{pmatrix}, \quad (31)$$

where ϵ is the imperfection of the transmission ratio. Then the unitary transformation matrix for an imperfect Mach-Zehnder interferometer becomes

$$\hat{U}_{\mathrm{MZI}} = \hat{U}_{\mathrm{BS}}\hat{U}_\phi\hat{U}_{\mathrm{BS}} = \begin{pmatrix} \frac{e^{i(\pi-\Delta\phi)}(1+\epsilon)^2+1}{\epsilon^2+2\epsilon+2} & \frac{i(1+\epsilon)(1-e^{i(\pi-\Delta\phi)})}{\epsilon^2+2\epsilon+2} \\ \frac{i(1+\epsilon)(e^{i(\pi-\Delta\phi)}-1)}{\epsilon^2+2\epsilon+2} & \frac{(1+\epsilon)^2+e^{i(\pi-\Delta\phi)}}{\epsilon^2+2\epsilon+2} \end{pmatrix}. \quad (32)$$

For any one of the four Mach-Zehnder interferometers (MZIs), it acts as the unitary mode transformation matrix $\hat{U}_{\mathrm{MZI}}$ on two of the spatial modes and leaves the other two unaffected. Here, for simplicity, we assume that all four MZIs have the same phase mismatches and that all eight beam splitters have the same parameter for imperfect transmission rate. Thus, we could write out four four-level unitary matrices that correspond to four MZIs and multiply them together to get the overall mode transformation matrix. The fidelity of the SWAP gate differs slightly for different input states, but all of the input states have an overall fidelity slightly higher than the lower bound:

$$\mathcal{F}_{\mathrm{SWAP}} > \left|\left(\frac{i(1+\epsilon)(1-e^{i(\pi-\Delta\phi)})}{2+2\epsilon+\epsilon^2}\right)^4\right|^2. \quad (33)$$

Note that the fidelity of all the input states is in the form of $x + \zeta y$, where x corresponds to the probability of the case in which the gate works as expected and ζy corresponds to the

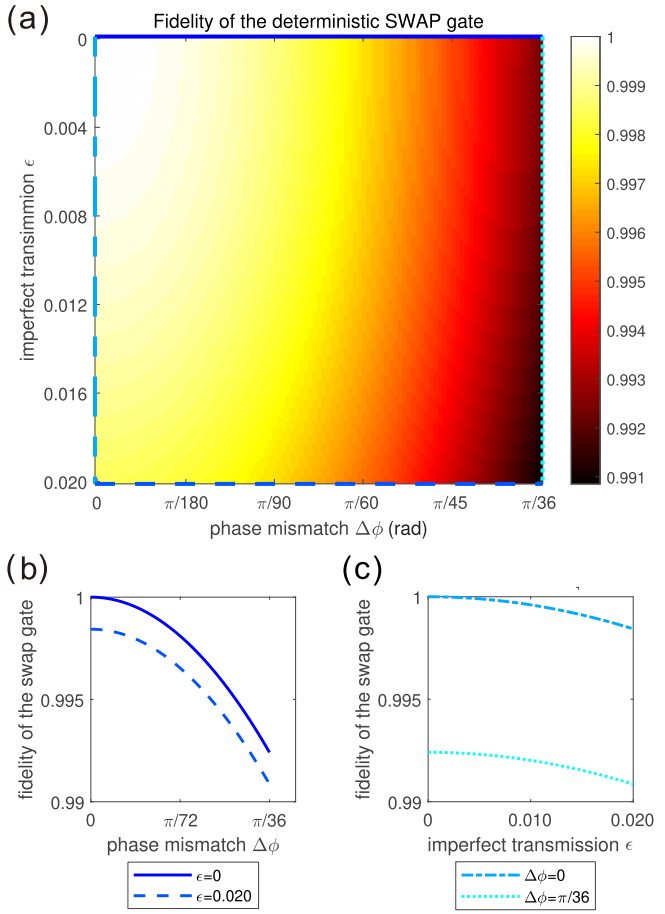

FIG. 5. (a) The fidelity map of the deterministic SWAP gate that is being inserted to perform a controlled-SWAP operation. From numerical calculations, the SWAP gate will always have a high fidelity above 99% under realistic conditions ($\epsilon \leqslant 0.02, \Delta\phi \leqslant \pi/36$). (b) The cross section of the fidelity map displaying the relationship between the fidelity of the SWAP gate and the phase mismatch of the two arms of the Mach-Zehnder interferometer, when the imperfect transmission parameter is set to be $\epsilon = 0, 0.02$. (c) The cross section of the fidelity map displaying the relationship between the fidelity and imperfect transmission parameter of the 50:50 beam splitter, when the phase mismatch is set to be $\Delta\phi = 0, \pi/36$.

probability of the case in which the gate experiences errors on both photons and gives out the expected result by accident. For example, if the input state is $|\varphi_{\text{in}}\rangle = |11\rangle = \hat{a}^\dagger\hat{c}^\dagger|\text{vac}\rangle$, it is most likely that the SWAP gate works as expected and switches the photon in spatial modes $a \to c$ and $c \to a$; however, both photons may experience errors simultaneously so that the locations of both photons remain the same, i.e., $a \to a$ and $c \to c$. In these two cases, both will give the correct output state, but the probability of the latter case is almost negligible, so we only take the first case into account. From (33), the overall fidelity of the deterministic SWAP gate is shown in Fig. 5.

C. Imperfections due to the calcite beam combiner

For the sake of simplicity, assume that the extinction ratio of the second calcite beam displacer is also r; the unitary mode transformation matrix of the second calcite beam displacer should be ideally the inverse matrix to the first one rotated by 90°,

$$\hat{U}_{r_2} = \frac{1}{\sqrt{1+r}}\begin{pmatrix} 1 & \sqrt{r}^* \\ -\sqrt{r} & 1 \end{pmatrix}. \tag{34}$$

In this step, we do not consider the angle of deviation of the mirror mounts for a second time because the calcite beam displacer and combiner are usually assembled together with the same orientation. By the definition of fidelity,

$$\mathcal{F}_3 = |\langle\varphi_{\text{real}}|\varphi_{\text{expected}}\rangle|^2 = \left|\frac{1}{1+r}\right|^2. \tag{35}$$

D. Overall fidelity of the proposed quantum Fredkin gate

For the input states $|000\rangle$, $|001\rangle$, $|010\rangle$, $|011\rangle$, the two photons will only enter at the calcite beam displacer and exit at the calcite beam combiner, so there may be three sources of error: angle of deviation of the gate as a whole, the extinction ratio of the calcite beam displacer, and the extinction ratio of the calcite beam combiner which was assumed to be the same as that of the calcite beam displacer. All of the sources of error only affect the polarization state of the two photons but not the spatial information, so the second and third logical qubits will still be correct. The overall fidelity is determined by multiplying the probability for each of the independent events together,

$$\begin{aligned}\mathcal{F}_{000} &= \mathcal{F}_{001} = \mathcal{F}_{010} = \mathcal{F}_{011} = \mathcal{F}_1\mathcal{F}_3 \\ &= \left|\frac{1}{1+r}(\cos\theta - \sqrt{r}\sin\theta)^2\right|^2\left|\frac{1}{1+r}\right|^2.\end{aligned} \tag{36}$$

For the input states $|100\rangle$, $|101\rangle$, $|110\rangle$, $|111\rangle$, an additional source of error is the crosstalk of the SWAP gate,

$$\begin{aligned}\mathcal{F}_{100} = \mathcal{F}_{101} = \mathcal{F}_{110} = \mathcal{F}_{111} &= \mathcal{F}_1\mathcal{F}_3\mathcal{F}_{\text{SWAP}} \\ &= \left|\frac{1}{1+r}(\cos\theta - \sqrt{r}\sin\theta)^2\right|^2 \times \left|\frac{1}{1+r}\right|^2 \\ &\quad \times \left|\left(\frac{i(1+\epsilon)(1-e^{i(\pi-\Delta\phi)})}{2+2\epsilon+\epsilon^2}\right)^4\right|^2.\end{aligned} \tag{37}$$

Based on (36) and (37), the lower bound of the overall fidelity of the controlled-SWAP gate is shown in Fig. 6.

E. Errors introduced by realistic detectors

Following [31], we will model a real detector with two parameters: a quantum efficiency η and a dark count rate λ. We will assume that the dark counts follow a Poisson distribution, so the probability of having d dark counts during the measurement interval τ will be

$$D(d) = e^{-\lambda\tau}\frac{(\lambda\tau)^d}{d!}. \tag{38}$$

We can then write the conditional probability of measuring k photons when l photons are presented as

$$P_D(k|l) = \sum_{d=0}^{k} D(k-d)\binom{l}{d}\eta^d(1-\eta)^{l-d}. \tag{39}$$

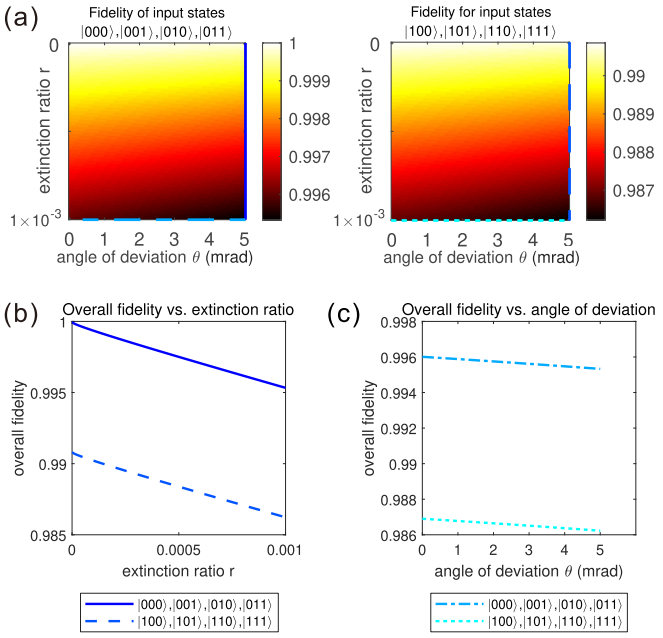

FIG. 6. (a) The overall fidelity map of the proposed quantum Fredkin gate. The fidelity for input states $|100\rangle$, $|101\rangle$, $|110\rangle$, $|111\rangle$ is lower due to the insertion of the SWAP gate. Assuming a perfect input state, the proposed controlled-SWAP gate will always have a high fidelity above 98.6% under realistic conditions ($\Delta\phi = \pi/36, \epsilon = 0.02, r \leqslant 1 \times 10^{-3}, \theta \leqslant 5 \times 10^{-3}$ rad). (b) The cross section of the fidelity map showing the relationship between overall fidelity and the extinction ratio of the calcite crystals, when the angle of deviation of the mirror is set to be $\theta = 5 \times 10^{-3}$ rad. (c) The cross section of the fidelity map displaying the relationship between overall fidelity and the angle of deviation of the kinematic mirror mounts, when the extinction ratio of the calcite crystals is set to be $r = 1 \times 10^{-3}$.

The overall probability of success at detection stage is thus given by

$$P_{\text{suc}} = P_D(1|1)^2 P_D(0|0)^6 = e^{-6\lambda\tau}[\lambda\tau e^{-\lambda\tau}(1-\eta) + e^{-\lambda\tau}\eta]^2. \quad (40)$$

For the avalanche photodiode, assume that $\eta = 0.8$, $\lambda\tau = 10^{-7}$; then the probability of a successful readout for the proposed controlled-SWAP gate is $P_{\text{suc}} = 0.64$.

F. Hong-Ou-Mandel interference

During the state-preparation stage in Fig. 4(a), we will not encounter the two-photon Hong-Ou-Mandel interference [32] since there is exactly one photon that is incident on each beam splitter. The Hong-Ou-Mandel interference can only take place inside the SWAP gate in Fig. 4(c). If the two photons are incident on different input ports of a 50:50 beam splitter, Hong-Ou-Mandel interference occurs, temporarily creating a quantum NOON state with two photons occupying one of the two spatial modes. However, when the two photons are incident again on the next 50:50 beam splitter with both of them entering from one input port, the two photons will separate at the two output ports.

Take the input state $|\phi_1\rangle = |010\rangle = \hat{a}_H^\dagger \hat{d}_H^\dagger |\text{vac}\rangle$ for example: two-photon Hong-Ou-Mandel interference will only occur at the last Mach-Zehnder interferometer. The quantum state is transformed into $|\phi_2\rangle = (\hat{b}_H^\dagger \hat{b}_H^\dagger - \hat{c}_H^\dagger \hat{c}_H^\dagger)|\text{vac}\rangle$ after the first beam splitter and then $|\phi_3\rangle = \hat{b}_H^\dagger \hat{c}_H^\dagger |\text{vac}\rangle$ after the second beam splitter. Therefore, the quantum NOON state will only exist within the four Mach-Zehnder interferometers in Fig. 4(c) and thus will not interfere with the readout process of the proposed controlled-SWAP gate.

G. Limitations

Although the controlled-SWAP gate in our proposal is resource efficient and feasible to implement, it does have certain limitations. In the next section, I will introduce the corresponding single-qubit gates of the proposed Fredkin gate, and we will see that the probabilistic nature of certain single-qubit gates on the control qubit is slightly problematic, considering they are normally given for free with other linear-optical quantum computing schemes.

Also, only a certain class of two-qubit and three-qubit operations is allowed in our proposal. Fortunately, these are the ones sufficient for the universal quantum computing when assisted by arbitrary one-qubit gates [17,18,33,34].

V. CORRESPONDING SINGLE-QUBIT GATES

In our proposal, single-qubit gates on the target qubits are simple since they are encoded in dual rails: phase shifters and beam splitters between two spatial modes are sufficient for arbitrary single-qubit operations. Single-qubit gates performed on the control qubit are feasible, but some of them require postselection and are thus probabilistic. This stems from the fact that our generic qubit states are entangled and unless the entanglement is generated at the state-preparation stage, it needs to be manipulated using measurement-induced nonlinearities as we only use linear-optical elements. On the other hand, single-qubit operations performed on target qubits can be achieved simply by means of linear interferometry.

First off, certain single-qubit gates such as the Pauli-Z gate and Pauli-X gate are easily realized with half-wave plates or phase shifters on the rails, as shown in Figs. 7(a) and 7(b).

In quantum circuits utilizing control gates, the control qubits are often prepared in superposition states achieved by using the Hadamard gate on a control qubit in the first place. In our proposal, this can be achieved by means of state preparation: we may prepare the initial state as $(|HH\rangle + |VV\rangle)/\sqrt{2}$ via a nonlinear process. This is not a universal Hadamard gate that can be inserted into the circuits, but it is useful for the applications introduced in Sec. VI.

We then discuss possible ways for constructing a heralded nondeterministic Hadamard gate on the control qubit. We first map the general polarization-entangled state $\alpha|HH\rangle + \beta|VV\rangle$ to a separable state $(\alpha|H\rangle + \beta|V\rangle) \otimes |H\rangle$ by applying a photonic controlled-NOT operation for polarization qubits. Then, we rotate the first photon by an arbitrary angle with a half-wave plate to obtain a new separable state $(\gamma|H\rangle + \delta|V\rangle) \otimes |H\rangle$. Finally, we apply another controlled-NOT operation for the polarization qubits to transform the separable state to a new entangled state $\gamma|HH\rangle + \delta|VV\rangle$. This controlled-NOT gate for polarization qubits is feasible but slightly difficult to implement both in free space [35], with the use of an

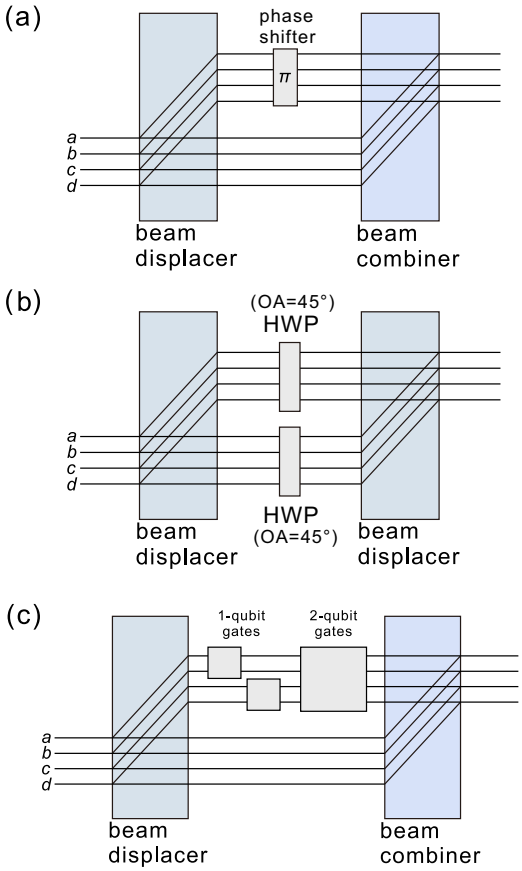

FIG. 7. (a) Implementation of the Pauli-Z gate on the control qubit. Note that the second calcite crystal is rotated by 90 degrees with respect to the first one. (b) Implementation of the Pauli-X gate on the control qubit. Note that the second calcite crystal in this case will be at the same orientation as the first one. (c) In the case of the Fredkin gate, a two-qubit SWAP gate should be inserted between the two calcite crystals. In other cases, arbitrary one-qubit and two-qubit gates on the target qubit(s) can be readily inserted and implemented since the dual-rail qubit(s) are compatible with the KLM protocol [8].

entangled ancillary pair of photons and postselection, and on chip [9], with the integration of partially polarizing beam splitters. Note that this probabilistic controlled-NOT gate is different from the controlled-NOT gate in our proposal since it does not involve multiple degrees of freedom.

The controlled-NOT gate used in the above process can be done much in the same way with some minor modifications and a theoretical success probability of $\frac{1}{4}$ [35] for our encoding scheme. Therefore, the Hadamard gate on the control qubit will have a successive probability of $\frac{1}{16}$. Though it can be improved to close to one with near-deterministic teleportation [31], the sophisticated resources demanded would be inconsistent with the simple implementations of the other gates in our proposal. Fortunately, the first Hadamard gate can always be achieved by means of state preparation, and it may already suffice in many applications where the most critical utilization of a Hadamard gate is within the preparation of an initial superposition state.

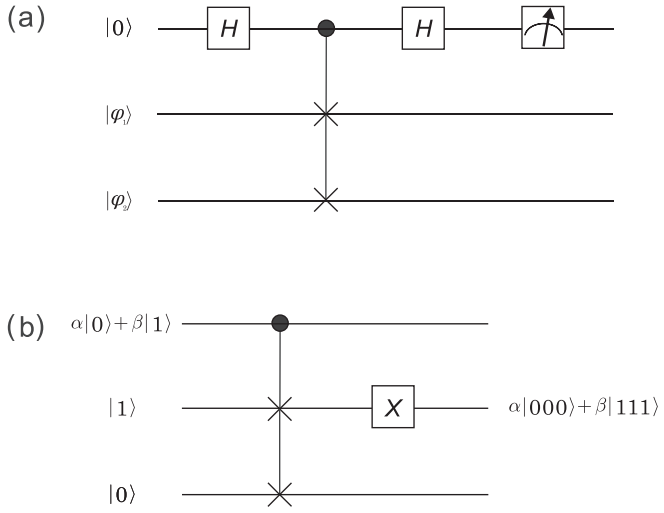

FIG. 8. (a) Schematic for the quantum swap test with the proposed Hadamard and controlled-SWAP gate. (b) Schematic for preparing generalized Greenberger-Horne-Zeilinger state involving the polarization and spatial degrees of freedom of the two photons.

VI. FURTHER APPLICATIONS

When working with quantum information, the question often arises of whether or not two states $|\varphi_1\rangle$ and $|\varphi_2\rangle$ are equal. The quantum Fredkin gate in our proposal may be readily used for a swap test [36], a procedure in quantum computation that is used to check how much two quantum states differ. The quantum circuit for the swap test is shown in Fig. 8(a). The first Hadamard gate can be achieved by means of state preparation since the desired output state is $(|HH\rangle + |VV\rangle)/\sqrt{2}$; similarly, the second Hadamard gate can be achieved by the method described in the previous section with a success probability $P = \frac{1}{16}$. From [36], we can find the probability of passing the swap test (finding the first qubit in $|0\rangle$) to be

$$P_p = \frac{1 + |\langle\varphi_1|\varphi_2\rangle|^2}{2}. \tag{41}$$

The probability of success for the swap test in our proposal is thus

$$P_s = PP_p = \frac{1 + |\langle\varphi_1|\varphi_2\rangle|^2}{32}. \tag{42}$$

Let us examine the evolution of both the polarization states and spatial rails of the two photons during the swap test, respectively. Consider a simple example where $|\varphi_1\rangle = |\varphi_2\rangle = |0\rangle$. The evolution through the circuit is

$$\xrightarrow{\text{state-preparation}} \frac{1}{\sqrt{2}}(\hat{b}_H^\dagger \hat{d}_H^\dagger + \hat{b}_V^\dagger \hat{d}_V^\dagger)|\text{vac}\rangle$$

$$\xrightarrow{\text{CSWAP}} \frac{1}{\sqrt{2}}(\hat{b}_H^\dagger \hat{d}_H^\dagger + \hat{b}_V^\dagger \hat{d}_V^\dagger)|\text{vac}\rangle$$

$$\xrightarrow{H} \hat{b}_H^\dagger \hat{d}_H^\dagger|\text{vac}\rangle.$$

In this case, the probability of success for the swap test is $P_s = \frac{1}{16}$, which is consistent with the theoretical prediction from (42) since $|\langle\varphi_1|\varphi_2\rangle|^2 = 1$ for two identical states.

Consider another example where $|\varphi_1\rangle = |0\rangle$, $|\varphi_2\rangle = |1\rangle$. The evolution through the circuit is

$$\xrightarrow{\text{state-preparation}} \frac{1}{\sqrt{2}}(\hat{b}_H^\dagger \hat{c}_H^\dagger + \hat{b}_V^\dagger \hat{c}_V^\dagger)|\text{vac}\rangle$$

$$\xrightarrow{\text{CSWAP}} \frac{1}{\sqrt{2}}(\hat{b}_H^\dagger \hat{c}_H^\dagger + \hat{d}_V^\dagger \hat{a}_V^\dagger)|\text{vac}\rangle$$

$$\xrightarrow{H} \frac{1}{2}(\hat{b}_H^\dagger \hat{c}_H^\dagger + \hat{b}_V^\dagger \hat{c}_V^\dagger + \hat{d}_H^\dagger \hat{a}_H^\dagger - \hat{d}_V^\dagger \hat{a}_V^\dagger)|\text{vac}\rangle.$$

The probability of success in this case is $P_s = \frac{1}{2} \times \frac{1}{16} = \frac{1}{32}$, which is consistent with the theoretical prediction from (42) since $|\langle\varphi_1|\varphi_2\rangle|^2 = 0$ for two orthogonal states.

Another interesting aspect related to the Fredkin gate is the possibility of creating hyperentangled states involving the polarization states and spatial degrees of freedom of the two photons, as shown in Fig. 8(b).

VII. CONCLUSION

In summary, we have proposed a general scheme for a family of deterministic linear-optical control gates, which are of high fidelity under realistic conditions, robust against photon loss, resource efficient, and relatively simple to implement in the laboratory. The proposed control gates, though requiring special state preparations and limited by the probabilistic nature of Hadamard gates on the control qubit, are indeed one of the solutions to the important and longstanding problem of how to achieve universal quantum computing using a resource operating at room temperature and widely accessible for photonic systems.

ACKNOWLEDGMENTS

I acknowledge fruitful discussions and useful guidelines from R. Chrapkiewicz as well as additional support from ViaX Research Institute in Beijing.

[1] M. A. Nielsen and I. L. Chuang, *Quantum Computation and Quantum Information* (Cambridge University Press, Cambridge, 2010), p. 676.

[2] F. Arute, K. Arya, R. Babbush, D. Bacon, J. C. Bardin, R. Barends, R. Biswas, S. Boixo, F. G. S. L. Brandao, D. A. Buell, B. Burkett, Y. Chen, Z. Chen, B. Chiaro, R. Collins, W. Courtney, A. Dunsworth, E. Farhi, B. Foxen, A. Fowler, C. Gidney, M. Giustina, R. Graff, K. Guerin, S. Habegger, M. P. Harrigan, M. J. Hartmann, A. Ho, M. Hoffmann, T. Huang, T. S. Humble, S. V. Isakov, E. Jeffrey, Z. Jiang, D. Kafri, K. Kechedzhi, J. Kelly, P. V. Klimov, S. Knysh, A. Korotkov, F. Kostritsa, D. Landhuis, M. Lindmark, E. Lucero, D. Lyakh, S. Mandrà, J. R. McClean, M. McEwen, A. Megrant, X. Mi, K. Michielsen, M. Mohseni, J. Mutus, O. Naaman, M. Neeley, C. Neill, M. Y. Niu, E. Ostby, A. Petukhov, J. C. Platt, C. Quintana, E. G. Rieffel, P. Roushan, N. C. Rubin, D. Sank, K. J. Satzinger, V. Smelyanskiy, K. J. Sung, M. D. Trevithick, A. Vainsencher, B. Villalonga, T. White, Z. J. Yao, P. Yeh, A. Zalcman, H. Neven, and J. M. Martinis, Quantum supremacy using a programmable superconducting processor, Nature (London) **574**, 505 (2019).

[3] C. R. Myers and R. Laflamme, Linear optics quantum computation: An overview, *Lecture notes for the International School of Physics "Enrico Fermi" on "Quantum Computers, Algorithms and Chaos", Varenna, Italy, July*, 2005.

[4] S. H. Tan and P. P. Rohde, The resurgence of the linear optics quantum interferometer – Recent advances and applications, Rev. Phys. **4**, 100030 (2019).

[5] H. S. Zhong, H. Wang, Y. H. Deng, M. C. Chen, L. C. Peng, Yi H. Luo, J. Qin, D. Wu, X. Ding, Y. Hu, P. Hu, X. Y. Yang, W. J. Zhang, H. Li, Y. Li, X. Jiang, L. Gan, G. Yang, L. You, Z. Wang, L. Li, N. L. Liu, C. Y. Lu, and J. W. Pan, Quantum computational advantage using photons, Science **370**, 1460 (2020).

[6] D. Leibfried, B. DeMarco, V. Meyer, D. Lucas, M. Barrett, J. Britton, W. M. Itano, B. Jelenković, C. Langer, T. Rosenband, and D. J. Wineland, Experimental demonstration of a robust, high-fidelity geometric two ion-qubit phase gate, Nature (London) **422**, 412 (2003).

[7] J. H. Plantenberg, P. C. De Groot, C. J. P. M. Harmans, and J. E. Mooij, Demonstration of controlled-NOT quantum gates on a pair of superconducting quantum bits, Nature (London) **447**, 836 (2007).

[8] E. Knill, R. Laflamme, and G. J. Milburn, A scheme for efficient quantum computation with linear optics, Nature (London) **409**, 46 (2001).

[9] A. Crespi, R. Ramponi, R. Osellame, L. Sansoni, I. Bongioanni, F. Sciarrino, G. Vallone, and P. Mataloni, Integrated photonic quantum gates for polarization qubits, Nat. Commun. **2**, 566 (2011).

[10] J. M. Lukens and P. Lougovski, Frequency-encoded photonic qubits for scalable quantum information processing, Optica **4**, 8 (2017).

[11] K. R. Motes, A. Gilchrist, J. P. Dowling, and P. P. Rohde, Scalable Boson Sampling with Time-Bin Encoding Using a Loop-Based Architecture, Phys. Rev. Lett. **113**, 120501 (2014).

[12] A. Babazadeh, M. Erhard, F. Wang, M. Malik, R. Nouroozi, M. Krenn, and A. Zeilinger, High-Dimensional Single-Photon Quantum Gates: Concepts and Experiments, Phys. Rev. Lett. **119**, 180510 (2017).

[13] N. J. Cerf, C. Adami, and P. G. Kwiat, Optical simulation of quantum logic, Phys. Rev. A **57**, R1477(R) (1998).

[14] J. C. Howell and J. A. Yeazell, Reducing the complexity of linear optics quantum circuits, Phys. Rev. A **61**, 052303 (2000).

[15] P. C. Humphreys, B. J. Metcalf, J. B. Spring, M. Moore, X. M. Jin, M. Barbieri, W. S. Kolthammer, and I. A. Walmsley, Linear Optical Quantum Computing in a Single Spatial Mode, Phys. Rev. Lett. **111**, 150501 (2013).

[16] B. G. Englert, C. Kurtsiefer, and H. Weinfurter, Universal unitary gate for single-photon two-qubit states, Phys. Rev. A **63**, 032303 (2001).

[17] A. Barenco, C. H. Bennett, R. Cleve, D. P. Divincenzo, N. Margolus, P. Shor, T. Sleator, J. A. Smolin, and H. Weinfurter, Elementary gates for quantum computation, Phys. Rev. A **52**, 3457 (1995).

[18] M. J. Bremner, C. M. Dawson, J. L. Dodd, A. Gilchrist, A. W. Harrow, D. Mortimer, M. A. Nielsen, and T. J. Osborne, Practical Scheme for Quantum Computation with Any Two-Qubit Entangling Gate, Phys. Rev. Lett. **89**, 247902 (2002).

[19] G. J. Milburn, Quantum Optical Fredkin Gate, Phys. Rev. Lett. **62**, 2124 (1989).

[20] D. E. Chang, V. Vuletić, and M. D. Lukin, Quantum nonlinear optics - Photon by photon, Nat. Photon. **8**, 685 (2014).

[21] J. Fiurášek, Linear-optics quantum Toffoli and Fredkin gates, Phys. Rev. A **73**, 062313 (2006).

[22] Y. X. Gong, G. C. Guo, and T. C. Ralph, Methods for a linear optical quantum Fredkin gate, Phys. Rev. A **78**, 012305 (2008).

[23] M. Fiorentino and F. N. C. Wong, Deterministic Controlled-NOT Gate For Single-Photon Two-Qubit Quantum Logic, Phys. Rev. Lett. **93**, 070502 (2004).

[24] L.-P. Deng, H. Wang, and K. Wang, Quantum CNOT gates with orbital angular momentum and polarization of single-photon quantum logic, J. Opt. Soc. Am. B **24**, 2517 (2007).

[25] Q. Zeng, T. Li, X. Song, and X. Zhang, Realization of optimized quantum controlled-logic gate based on the orbital angular momentum of light, Opt. Express **24**, 8186 (2016).

[26] S. Y. Baek and Y. H. Kim, Spectral properties of entangled photon pairs generated via frequency-degenerate type-I spontaneous parametric down-conversion, Phys. Rev. A **77**, 043807 (2008).

[27] P. Kultavewuti, E. Y. Zhu, X. Xing, L. Qian, V. Pusino, M. Sorel, and J. S. Aitchison, Polarization-entangled photon pair sources based on spontaneous four wave mixing assisted by polarization mode dispersion, Sci. Rep. **7**, 5785 (2017).

[28] H. Terashima, S. Kobayashi, T. Tsubakiyama, and K. Sanaka, Quantum interferometric generation of polarization entangled photons, Sci. Rep. **8**, 15733 (2018).

[29] A. B. Bozkurt and S. Kocaman, Linear optical deterministic and reconfigurable SWAP gate (unpublished).

[30] J. C. Campbell, S. Demiguel, F. Ma, A. Beck, X. Guo, S. Wang, X. Zheng, X. Li, J. D. Beck, M. A. Kinch, A. Huntington, L. A. Coldren, J. Decobert, and N. Tscherptner, Recent advances in avalanche photodiodes, IEEE J. Select. Top. Quantum Electron. **10**, 777 (2004).

[31] F. Spedalieri, H. Lee, and J. Dowling, Linear Optical Quantum Computing with Polarization Encoding, in *Frontiers in Optics, OSA Technical Digest Series* (Optica Publishing Group, 2005), paper LMB4.

[32] L. Mandel, C. K. Hong, and Z. Y. Ou, Measurement of Subpicosecond Time Intervals between Two Photons by Interference, Phys. Rev. Lett. **59**, 2044 (1987).

[33] D. P. DiVincenzo, Two-bit gates are universal for quantum computation, Phys. Rev. A **51**, 1015 (1995).

[34] S. Lloyd, Almost Any Quantum Logic Gate is Universal, Phys. Rev. Lett. **75**, 346 (1995).

[35] S. Gasparoni, J. W. Pan, P. Walther, T. Rudolph, and A. Zeilinger, Realization of a Photonic Controlled-NOT Gate Sufficient for Quantum Computation, Phys. Rev. Lett. **93**, 020504 (2004).

[36] J. C. Garcia-Escartin and P. Chamorro-Posada, Swap test and Hong-Ou-Mandel effect are equivalent, Phys. Rev. A **87**, 052330 (2013).